

Comparison of techniques to characterise the point spread function of an acoustic-resolution photoacoustic microscope

Anant Shah, Aoife M. Ivory, Srinath Rajagopal, Bajram Zeqiri
Ultrasound and Underwater Acoustics, National Physical Laboratory, Teddington United Kingdom
Anant.Shah@npl.co.uk

Abstract— This work presents a method to characterise the photoacoustic (PA) point spread function (PSF) of an acoustic-resolution PA microscope (AR-PAM) (easyPAM-400™, Kibero). In the absence of a point absorber, the conventional lateral and axial PSF characterisation approaches of a PAM involve the line spread function (LSF) measurement of an edge and shift-and-sum method, respectively. A comparison is made between these approaches that derive the PSF to that obtained by imaging quasi point targets. The PA lateral and axial resolutions of the PAM derived using the approaches mentioned above were estimated to be $6.59 \pm 1.23 \mu\text{m}$ and $7.6 \pm 0.2 \mu\text{m}$, respectively. The lateral and axial PSF obtained from the point target were $7.75 \pm 0.25 \mu\text{m}$ and $8.3 \pm 0.67 \mu\text{m}$, respectively. Comparison indicated that there is good agreement between the approaches that derive the PSF and that obtained by imaging point targets.

Keywords— photoacoustic microscope, point spread function, line spread function, shift and sum.

I. INTRODUCTION

Photoacoustic imaging (PAI) is an imaging modality that combines the advantages of high optical contrast and spectral specificity of optical imaging with a good penetration depth of ultrasound imaging [1]. In PAI, a specimen of interest is illuminated using a sufficiently short laser pulse, that satisfies the stress and thermal confinement criteria. Chromophores present in the path of the scattered light absorb the light, undergo thermoelastic expansion and generate an acoustic wave that propagates to the surface and can be detected using an ultrasonic transducer [1]. The reconstructed photoacoustic (PA) image is based upon the distribution of optical absorption in the specimen of interest. In the last four decades, PAI has been used for several pre-clinical and clinical studies, demonstrating its potential in a range of biomedical applications [2].

For high resolution PAI at a microscopic level, two classes of photoacoustic microscopy (PAM) can be implemented: Acoustic-Resolution PAM (AR-PAM) and Optical-Resolution Microscopy (OR-PAM) [3]. The PA lateral resolution of AR-PAM is dependent on the characteristics of the ultrasound transducer (center frequency and numerical aperture), whereas for OR-PAM, the lateral resolution is dependent on the properties of the laser beam (wavelength and beam diameter). The PA axial resolution of both the systems is predominantly dependent on the imaging depth and frequency bandwidth of the ultrasound transducer [3]. AR-PAM has a relatively greater depth of imaging in comparison to OR-PAM due to lower depth dependent ultrasonic attenuation in comparison to optical

scattering. Depending on the nature of the application and desired resolution, either microscopy technique could be employed. Hybrid or switchable AR-PAM and OR-PAM microscopes have also been developed to take advantage of both the types of systems [4].

An accurate estimation of the PSF is critical in understanding the theoretical resolution limit of the PAM technique and identifying any problems caused by the PAM's calibration settings. Additionally, if known, the PSF can be used to recover the 'true' image by mathematical deconvolution of the recorded data [5]. Correct determination of the PSF is therefore fundamental for the application of deconvolution algorithms for an accurate image recovery of a PAM.

For any imaging system, the PSF can be traditionally determined by direct measurement of a system's response to a quasi-point source. However, in the absence of true point absorbers, simplified methods involving;

- Edge-spread function (ESF) and Line-spread function (LSF) measurements of a slanted edge [6]–[8] and
- Shift-and-Sum approach [6], [7], [9],

have been employed by research groups, to assess the PA lateral and axial resolution of a PAM, respectively. Whilst these approaches have been consistently used to characterize the PSF of a PAM, there is a clear need for quantitative evaluation of these approaches. The objective of this study is to make a comparison between the methods that derive the PSF of a PAM and gauge their accuracy to that obtained by imaging point targets.

II. MATERIALS AND METHODS

A. Acoustic-resolution Photoacoustic-microscope

Fig. 1a shows the schematic of an easyPAM™-400 microscope (Kibero, Germany). The system uses a single element, focused transducer (center frequency (F_c) = 400 MHz) for generation and reception of acoustic waves. The bandwidth (BW) of the transducer is 150 MHz, with an aperture angle (Θ) of 60° and a focal length of $30 \mu\text{m}$, as stated by the manufacturer. For PA acquisition, a specimen of interest is illuminated using laser pulses of 532 nm (pulse width – 1.3 ns) generated by a solid-state laser system (FDSS 532/1024-1000, CryLaS GmbH, Germany). The pulse energy is set to a maximum value of $150 \mu\text{J}$ with a repetition rate of 1 kHz. For broad beam illumination, the light is guided through an optical fiber which delivers the light onto the sample by using a ring illuminator (Fig. 1B). The

PA signals are amplified by a low noise 60 dB amplifier. Signal digitization is synchronized to the laser trigger, with an acquisition sampling rate up to 2 GHz/s using a 14-bit digitizer. Images were acquired by scanning the sample stage in a raster pattern (XY-scanner, Fig. 1A) through the target area.

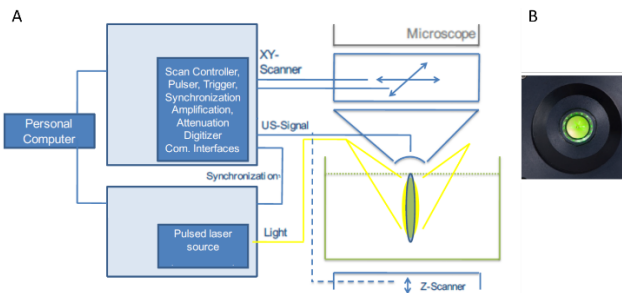


Fig. 1 A. Schematic of the easyPAM microscope. B. Image showing the easyPAM (400 MHz) lens and the ring illuminator delivering the 532 nm laser. Images courtesy of Kibero™.

B. Approaches for characterisation of lateral resolution

i. Theoretical lateral resolution

Theoretically, the lateral resolution of the AR-PAM is given by $0.71 \lambda/NA$ [3], where λ is the centre-frequency wavelength of the ultrasound transducer and NA is the numerical aperture. λ was calculated from the speed of sound in deionized water (v_s) and F_c , using the formula $\lambda = v_s / F_c$ and NA was calculated from the aperture angle, $NA = \sin(\Theta)$.

ii. USAF Resolution Test Target Imaging

An estimate of the acoustic and PA lateral resolution of the microscope was obtained by imaging a USAF 1951 test target (R1DS1P, Thorlabs). A $500 \mu\text{m} \times 500 \mu\text{m}$ area of the test target, covering group 6 and group 7 elements, was scanned in step-size of $1 \mu\text{m}$ in both X and Y directions, using the acoustic and PA modes of the microscope.

iii. ESF – LSF methodology

To estimate the lateral resolution of the PAM obtained using the ESF-LSF approach, a tilted USAF 1951 chart was scanned. 15 edges were selected in such a way that approximately half of each region of interest consisted of the PA signals of a target and the remainder half from the background. The ESFs of the edges were calculated using the QuickMTF software (v 2.12, [10]) and were fitted to an error function using MATLAB (R2017b, Mathworks). The LSFs were obtained by taking the first order derivative of the fitted ESFs. The full width at half maxima (FWHM) of the 15 LSFs were calculated to derive the lateral resolution of the PAM.

C. Approaches for characterisation of axial resolution

i. Theoretical axial resolution

The theoretical axial resolution was determined by acoustic parameters according to $0.88 * (v_s/BW)$ [3], where v_s is the speed of sound in deionized water, and BW is the frequency bandwidth of the ultrasound transducer.

ii. Shift and sum approach

A photoacoustic A-line signal was acquired from a glass slide coated with a gold film (thickness – 50 nm) at the focal position. The gold film was shifted in step sizes of $0.2 \mu\text{m}$ in a downward direction using the z-scanner (Fig. 1A), and A-line signals were acquired at each position. This process was repeated three times. The axial resolution was defined as the minimum shift-distance needed to differentiate the two peaks of the envelope of summed A-line signals (original and shifted), with an amplitude difference of greater than 10% [9]. The amplitude difference was the difference between the amplitude of the smaller of the two peaks in the enveloped signal and the trough between the two peaks. The % amplitude difference was plotted against the shifted distance to determine the axial resolution.

D. Imaging a quasi-point target

For comparing the derived PA lateral and axial resolution of the PAM to that obtained by imaging a point source, black dyed polystyrene microspheres (diameter - $3 \mu\text{m}$, PolySciences, USA) were used as imaging targets. The spheres were homogeneously dispersed in 10% gelatin (G2625, Sigma Aldrich). $100 \mu\text{L}$ of the suspension was pipetted onto a microscope glass slide, allowed to solidify at room temperature, and placed under the PAM. Three isolated microspheres were imaged using the system. Since the diameter of the microsphere was smaller than the expected PA lateral and axial resolution of the PAM, the FWHM of the gaussian fits of the lateral and axial spread profiles, extracted from the centre of the C-scan and the B-mode image respectively, gave the lateral and axial resolution of the PAM. The student's t-test was performed to assess the statistical significance of the difference between the resolutions obtained using imaging of the microspheres to the other techniques.

III. RESULTS

A. Characterisation of lateral resolution

i. Theoretical lateral resolution

The theoretical lateral resolution for the PAM, determined using the equation $(0.71 \lambda/NA)$, was estimated to be $3.1 \mu\text{m}$.

ii. USAF Resolution Test Target Imaging

As shown in Fig. 2, it was possible to resolve the elements in the target group 7 element 2 and target group 6 element 2 (red arrows, Fig. 2) in the acoustic and the PA images, respectively. The gaps between two absorptive bars were $3.48 \mu\text{m}$ and $6.96 \mu\text{m}$ in the acoustic and PA images, respectively. The acoustic lateral resolution was similar to the theoretical lateral resolution. As expected, the lateral resolution in the PA mode was lower than the predicted theoretical resolution and the acoustic resolution.

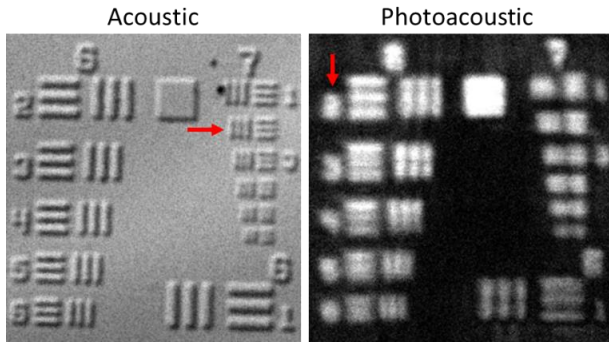


Fig. 2 Acoustic (left) and Photoacoustic (right) images of group 6 and group 7 elements of a 1951 USAF resolution test target. The red arrows indicate the element groups that could be resolvable using the PAM in the two modes.

iii. Edge spread function

For the tilted image, 15 edges were selected as shown in Fig. 3A (dotted boxes). The plots for error-function fitted ESFs and LSFs of the edges are shown in Fig. 3B. The lateral resolution, determined by estimating the FWHM of the LSF of the edges was estimated to be $6.59 \pm 1.23 \mu\text{m}$, well matching with the PA resolution estimated using the USAF target.

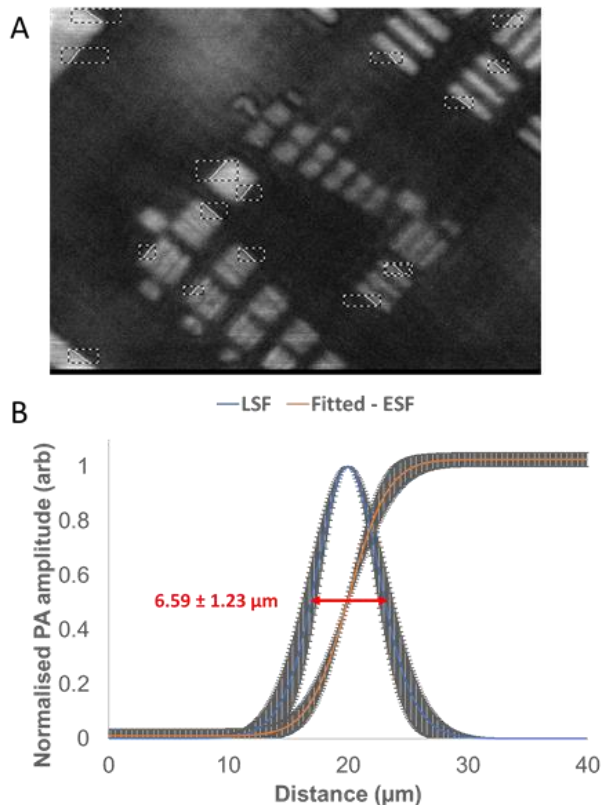


Fig. 3 A. Photoacoustic image of a tilted USAF-1951 resolution test target. The dotted line boxes in the image show the 15 edges that were analysed to obtain the ESF and LSF. B. Plots for error-function fitted ESFs (orange curve) and the LSFs (blue curve). The error bars show the standard deviation of 15 edges. The FWHM of the LSFs, indicated by the red line, was $6.59 \pm 1.23 \mu\text{m}$.

B. Characterisation of axial resolution

i. Theoretical axial resolution

The theoretical PA axial resolution for the easyPAM system, determined using the equation $(0.88 * (v_s/BW))$, was estimated to be $8.74 \mu\text{m}$.

ii. Shift and sum approach

Fig. 4A shows that the sum of the PA envelope of the two A-line signals (original and shifted) possesses two distinct peaks representing the gold film, when separated by $7.8 \mu\text{m}$. The minimal shifted distance that allows a resolution of the two peaks (by 10% amplitude difference), estimated to be $7.6 \pm 0.2 \mu\text{m}$, was considered as the resolution along the axial direction. Fig. 4B. shows the plot of % amplitude difference versus the shift distance and the red arrow indicates the shift distance at which the amplitude difference is significantly greater than 10% and continues to stay so, with further shift.

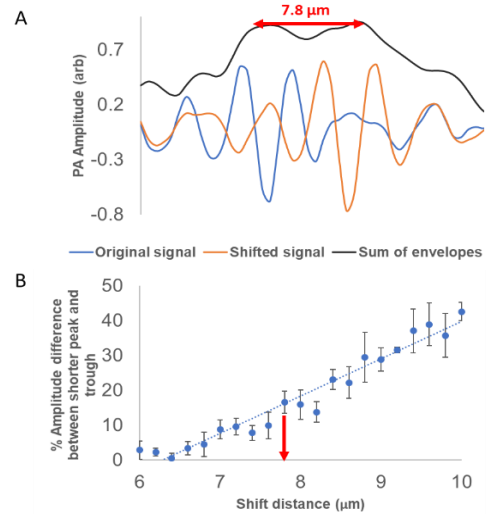


Fig. 4 A. Photoacoustic A-line signals, original (blue) and shifted (orange), $7.8 \mu\text{m}$. The black curve indicates the sum of the envelopes of the two signals, with two distinct peaks. B. A plot showing the relation of the percentage amplitude difference between the shorter peak and the trough, with the shift distance. The dotted blue line is a linear fit to the data points. The red arrow indicates the axial resolution of the system, estimated using the approach.

C. Imaging a quasi-point target

Fig. 5A and 5B show an isosurface rendering and central slices (x-y plane) of a polystyrene microsphere. As shown in Fig. 5C, the gaussian-fitted profile through the central slices of the microsphere have FWHM values of $7.73 \mu\text{m}$ and $8.99 \mu\text{m}$ along the lateral and axial directions, respectively. The blue dots in the plots are the experimental values and red solid line is the gaussian fit. The lateral and axial resolution obtained from the microsphere were $7.75 \pm 0.25 \mu\text{m}$ and $8.3 \pm 0.67 \mu\text{m}$, respectively. These values correspond well to the lateral resolution derived using the alternative approaches, as shown in Table 1. There was no statistically significant difference between the approaches that derive the PSF and that obtained by imaging point targets.

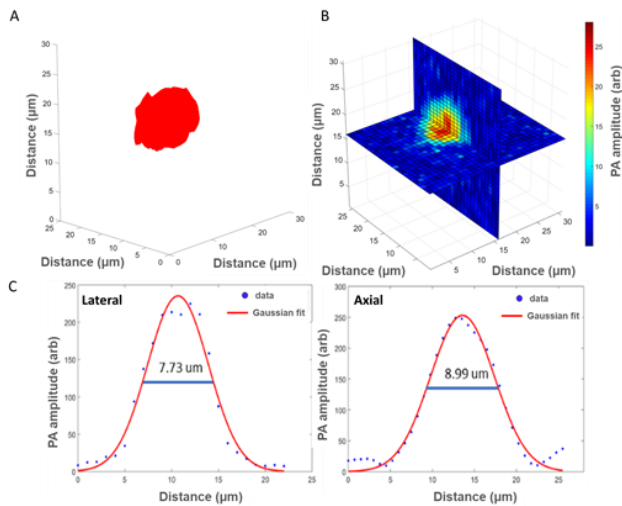


Fig. 5. A. Representative isosurface rendering of a microsphere, as imaged using the PAM. The vertical axis is the z-direction. B. Transverse slices (vertical and horizontal) passing through the center of the microsphere. The colour bar indicates the PA amplitude (arb). C. Plots of the gaussian-fitted (red line) lateral and axial profiles through the central slices of the microsphere shown in 5B. The mean FWHM for the three microspheres was calculated to be 7.75 μm and 8.3 μm , respectively.

TABLE I. COMPARISON OF ESTIMATES OF LATERAL AND AXIAL RESOLUTION OF THE AR-PAM USING DIFFERENT TECHNIQUES.

Lateral resolution (μm)	Theoretical	ESF-LSF	Quasi-point source
		3.1	6.59 ± 1.23
Axial Resolution (μm)	Theoretical	Shift-and-sum	Quasi-point source
		8.74	7.6 ± 0.2

IV. DISCUSSION & CONCLUSION

The objective of this work was to make a comparison between approaches that derive the PA PSF of an AR-PAM to that obtained by imaging a quasi-point target. It was observed that the PA lateral resolution of the AR-PAM (Fig. 2) was poorer than the acoustic resolution and the predicted theoretical PA lateral resolution of 3.1 μm , as expected. This could be due to clutter, arising from PA signals generated outside the imaging plane of the transducer [11], as a result of the broad-beam illumination of the laser. The PA lateral resolution of $6.59 \pm 1.23 \mu\text{m}$ obtained using the ESF-LSF approach, matched well to that estimated using the UASF resolution target (6.96 μm). The standard deviation ($\sim 19\%$) of the mean lateral resolution estimated using the ESF-LSF approach suggests the need to perform measurements on several edges at different angles, rather than utilising a single edge to characterise the lateral resolution of a PAM. There was no significant difference ($p < 0.05$) between the lateral PA resolution obtained using the ESF-LSF method and the quasi-point source imaging approach ($7.75 \pm 0.25 \mu\text{m}$).

The theoretical PA axial resolution of the PAM was estimated to be 8.74 μm . The shift and sum methodology suggest that the

PAM is capable of differentiating absorbers located $7.6 \pm 0.2 \mu\text{m}$, apart from each other. Moothanchery *et al.* [4] also observed that the axial resolution determined using the shift and sum approach (16.5 μm) was lower in comparison to the predicted axial resolution (29 μm) or the equivalent obtained using a point target (33 μm) for their hybrid PAM system. We observed a similar trend of the shift and sum approach estimating the axial resolution to be lower ($7.6 \pm 0.2 \mu\text{m}$) than the theoretical prediction (8.74 μm) and that obtained by imaging a single microsphere as an approximation to a point target ($8.3 \pm 0.67 \mu\text{m}$). However, this difference between the two approaches was not statistically significant ($p < 0.05$). Based on the results obtained in this study, it can be concluded that there is good agreement between the approaches that derive the PSF of an AR-PAM to that obtained by imaging quasi-point targets.

ACKNOWLEDGMENT

The U.K. Department for Business, Energy & Industrial Strategy’s funding of the National Measurement System is gratefully acknowledged.

REFERENCES

- [1] P. Beard, “Biomedical photoacoustic imaging,” *Interface Focus*, vol. 1, no. June, pp. 602–631, 2011.
- [2] J. L. Su *et al.*, “Advances in clinical and biomedical applications of photoacoustic imaging,” *Expert Opin. Med. Diagn.*, vol. 4, no. 6, pp. 497–510, 2010.
- [3] J. Yao and L. V Wang, “Photoacoustic Microscopy,” *Laser Photon. Rev.*, vol. 7, no. 5, p. 10, 2013.
- [4] M. Moothanchery and M. Pramanik, “Performance characterization of a switchable acoustic resolution and optical resolution photoacoustic microscopy system,” *Sensors*, vol. 17, no. 2, 2017.
- [5] D. Cai, Z. Li, and S.-L. Chen, “In vivo deconvolution acoustic-resolution photoacoustic microscopy in three dimensions,” *Biomed. Opt. Express*, vol. 7, no. 2, p. 369, 2016.
- [6] C. Zhang *et al.*, “Reflection-mode submicron-resolution in vivo photoacoustic microscopy,” *J. Biomed. Opt.*, vol. 17, no. 2, p. 020501, 2012.
- [7] T. Wang *et al.*, “All-optical photoacoustic microscopy based on plasmonic detection of broadband ultrasound,” *Appl. Phys. Lett.*, vol. 107, no. 15, 2015.
- [8] M. Moothanchery, R. Bi, J. Y. Kim, S. Jeon, C. Kim, and M. Olivo, “Optical resolution photoacoustic microscopy based on multimode fibers,” *Biomed. Opt. Express*, vol. 9, no. 3, p. 1190, 2018.
- [9] Z. Xie, S. Jiao, H. F. Zhang, and C. A. Puliafito, “Laser-scanning optical-resolution photoacoustic microscopy,” *Opt. Lett.*, vol. 34, no. 12, pp. 1771–1773, 2009.
- [10] O. Kurtsev, “<http://www.quickmtf.com/>,” *Last accessed on 20th August 2019*.
- [11] M. Jaeger, “Deformation-compensated averaging for clutter reduction in epiphotoacoustic imaging in vivo,” *J. Biomed. Opt.*, vol. 17, no. 6, p. 066007, 2012.